Materials Today Communications 56 (2026) 116069

Contents lists available at ScienceDirect

Materials Today Communications

journal homepage: www.elsevier.com/locate/mtcomm

ANN-based prediction of thermo-hydraulic performance of MgO and MgO–CuO transformer oil nanofluids in a plate-fin heat exchanger

Narinderjit Singh Sawaran Singh [a], Abdalmalik N. Attallah [b], Muntadher Abed Hussein [c], Mithaq Nazar Jassim [d], Ahmed Najat Ahmed [e], Hakim AL Garalleh [f], Zuhair Jastaneyah [g], Mahmut Taner [h,*], Soheil Salahshour [i,j,k,l]

[a] Faculty of Data Science and Information Technology, INTI International University, Persiaran Perdana BBN, Putra Nilai, Nilai 71800, Malaysia
[b] Department of Power Mechanical Engineering Techniques, College of Engineering Technologies, University of Al Maarif, Al Anbar 31001, Iraq
[c] University of Manara, Amarah, Maysan, Iraq
[d] Al-Amarah University College, Maysan, Iraq
[e] Department of Information Technology, College of Engineering and Computer Science, Lebanese French University, Erbil, Kurdistan Region, Iraq
[f] Department of Mathematical Science, College of Engineering, University of Business and Technology, Jeddah 21361, Saudi Arabia
[g] Department of Mechanical Engineering, College of Engineering, University of Business and Technology, Jeddah 21361, Saudi Arabia
[h] Faculty of Engineering and Architecture, Istanbul Gelisim University, Istanbul, Turkey
[i] Faculty of Engineering and Natural Sciences, Istanbul Okan University, Istanbul, Turkey
[j] Faculty of Engineering and Natural Sciences, Bahcesehir University, Istanbul, Turkey
[k] Research Center of Applied Mathematics, Khazar University, Baku, Azerbaijan
[l] Faculty of Science and Letters, Piri Reis University, Tuzla, Istanbul, Turkey

ARTICLE INFO

Keywords:
Thermo-hydraulic properties
Transformer oil
Heat exchanger
Hybrid nanofluid
Artificial neural networks
Inclusive innovation

ABSTRACT

Accurate prediction of the coupled thermal and hydraulic behaviors of nanofluids in heat exchangers potentially avoids repetitive experimental testing. Thus, the present study aimed to develop a data-driven surrogate modeling framework capable of predicting the thermal and hydraulic behaviors of MgO and MgO-CuO / Transformer Oil nanofluids in a plate-fin heat exchanger in a temperature range of 30–70 °C. We digitized literature-sourced data using WebPlotDigitizer and reconstructed heat transfer and flow-rate experimental curves with piecewise cubic Hermite interpolation, maintaining monotonic behavior in the time dimension. Four independent forward feedforward 2–5–1 architecture artificial multilayer perceptrons, trained using the Levenberg-Marquardt technique, predicted overall and convective heat transfer coefficients, Reynolds number, and pumping power. Reliability was demonstrated through 30 individual runs, 10-fold cross-validation, repeat internal holdout, grouped anchor holdout, and boundary stress tests. The results were compared with support vector regression with radial basis function (SVR-RBF), random forest regression (RFR), and a multilayer perceptron trained via stochastic gradient descent with momentum. The overall percentage error (mean absolute error, MAE) for the four parameters for the Levenberg-Marquardt approach was 2.363, 0.433, 1.055, and 0.280%; the mean coefficient of determination (R2) ranged from 0.97838 to 0.99789. No approach dominated overall; alternative models had minimal training error for individual output variables, while the Levenberg-Marquardt framework produced the most evenly distributed results and the lowest variability among the four coupled responses. Under boundary evaluation, this framework captured the highest overall efficiency (lowest root mean square errors for both the convective heat transfer coefficient, 25.491 $W/m^2 \cdot K$, and the Reynolds number, 21.653). Under the given boundary conditions, changes in oil viscosity due to heat input altered hydraulic flow-rate behavior, while adding nanoparticles changed thermal efficiency and the pumping energy cost ratio. By integrating multiple response models, comparing algorithms, and using a boundary-validation approach, the constructed framework may provide very fast intra-domain filtering of the thermo-hydraulic design. Nevertheless, its usability is limited to the described test conditions for the mentioned fluid and exchanger type.

* Corresponding author.
E-mail addresses: mtaner340@gmail.com, mtaner@gelisim.edu.tr (M. Taner).

https://doi.org/10.1016/j.mtcomm.2026.116069
Received 29 July 2026; Received in revised form 30 August 2026; Accepted 3 September 2026
Available online 8 September 2026

Nomenclature

Symbol	Definition, Unit
b_h	Hidden-layer bias vector, Dimensionless
b_o	Output-layer bias, Dimensionless
e_i	Prediction error for the ith sample, Same as the corresponding output
e	Vector of prediction errors, Same as the corresponding output
F(w)	Objective function minimized during network training, Output-dependent squared unit
H	Approximate Hessian matrix, Dimensionless after normalization
I	Identity matrix, Dimensionless
J	Jacobian matrix of network errors, Dimensionless after normalization
m	Number of training samples, Dimensionless
n	Total number of evaluated samples, Dimensionless
R	Correlation coefficient, Dimensionless
R^2	Coefficient of determination, Dimensionless
Re	Reynolds number, Dimensionless
T	Operating temperature, °C
w	Vector of network weights and biases, Dimensionless
w_{ij}	Weight connecting the input and hidden layers, Dimensionless
w_{jo}	Weight connecting the hidden and output layers, Dimensionless
x_1	Normalized temperature input, Dimensionless
x_2	Numerically encoded nanofluid-structure input, Dimensionless
y_i	Reference value of the ith sample, Same as the corresponding output
$\hat{y}_i$	ANN-predicted value of the ith sample, Same as the corresponding output
$\bar{y}$	Mean of the reference values, Same as the corresponding output
$\bar{\hat{y}}$	Mean of the ANN-predicted values, Same as the corresponding output

Greek symbols

Symbol	Definition, Unit
λ	Levenberg–Marquardt damping parameter, Dimensionless

Abbreviations

Abbreviation	Definition, Unit, where applicable
AE	Absolute error, Same as the corresponding output
ANN	Artificial neural network, –
CHTC	Convective heat transfer coefficient, W m^{-2} K^{-1}
HNF	Hybrid nanofluid, –
HT	Heat transfer, –
LM	Levenberg–Marquardt, –
ML	Machine learning, –
MLP	Multilayer perceptron, –
MSE	Mean squared error, Output-dependent squared unit
NF	Nanofluid, –
NP	Nanoparticle, –
PP	Pumping power, W
RF	Random forest, –
RMSE	Root mean square error, Same as the corresponding output
SGD	Stochastic gradient descent, –
SVR	Support vector regression, –
UHTC	Overall heat transfer coefficient, W m^{-2} K^{-1}

1. Introduction

1.1. Motivation and engineering context

Plate-fin heat exchangers (PFHEs) are used in diverse applications, including power systems, auto-coolers, aircraft systems, refrigerating units, and small energy-conversion devices, because they achieve high HT capacity in a confined volume through very high surface-area density [1,2]. But the system efficiency was determined not just by heat transfer (HT) performance, but also by a rise in flow resistance and thus pressure loss and circulation energy that was conventionally accompanied by increasing the HT rate; such that a performance value based only on a thermal index may show itself very uneconomical when an analysis on the hydraulic penalty aspect was carried out [3,4]. In PFHEs, where long, narrow channels and repeated boundary-layer development through an arrangement of separated fins were inevitable, both thermal and hydraulic phenomena were highly sensitive to working-fluid properties and operating conditions [5–7]. Transformer cooling is an application where such trade-offs must be carefully managed: Transformer oil, besides its role in electrical insulation, also dissipates the power generated in windings and magnetic circuits. However, because of its thermal properties (comparatively poor thermal conductivity) and the tendency of oil viscosity to change with T, poor heat dissipation can easily lead to high-T hot spots and accelerate oil deterioration when the thermal load increases. By dispersing small solid particles (NPs) in it, the modified transport characteristics of the resulting nanofluid (NF) arose. However, combining two different types of NPs forms a hybrid nanofluid (HNF), whose advantages over mono-NF can be even more varied [8–11], for example concerning thermal conductivity, viscosity, and even interfacial energy transport, besides other important factors.

Nevertheless, enhanced HT ability of an NF did not ensure efficiency. Introducing particles, especially at concentrations that can significantly enhance thermal performance, can raise viscosity, while increasing T decreases viscosity; therefore, the relative contribution between thermal gain and circulation power changes, and an optimum solution might be available in the system. Consequently, evaluating NF-enhanced PFHEs is best approached through simultaneous measurements of both thermal and hydraulic performance. To be able to present diverse aspects of thermal-hydraulic behavior, some parameters must be measured for different values, such as UHTC representing combined thermal resistance, CHTC as convective heat transfer coefficient (CHTC) between flow and surface, Reynolds number (Re) denoting the relationship between inertia and viscous forces in a flow, and pump power (PP). Results obtained under certain operating conditions may not show the same trend across conditions because Reynolds number, CHTC, and UHTC depend nonlinearly on operating parameters, and boundary-layer properties change with different NP formulations, affecting pressure drop and, in turn, pump power.

1.2. Recent experimental and data-driven studies

A strong connection between NF composition and performance characteristics was evident in many experimental studies and optimization analyses in recent years. For instance, Tekir et al. [12] tested FeO/water and FeO-Cu/water HNFs in a plate heat exchanger and measured the impact of both fluid composition and external HT system parameters on effectiveness, Nusselt number (Nu), and CHTC concurrently. Patel et al. [13] presented experimental work in investigating the effect of Cu and AlO mono- and hybrid NFs within a square-pyramid solar still, determining that the AlO-Cu blend with an 80:20 ratio yielded the highest distilled output and efficiency values; there was clearly potential for proportions of different NPs to greatly affect a system's overall thermal behavior. Babaelahi et al. [14] studied a plate-tube and fin heat exchanger using multi-objective optimization, determining that system thermal improvement could only be taken in tandem with total volume and PP. Machine learning (ML) approaches, more specifically artificial neural networks (ANN), began to be used in analysis because more empirical thermal-hydraulic data are available for predicting fluid flow and HT behavior. For example, Aktas et al. [15] sought to use both experimental data and an ANN and a PINN to predict the Nusselt number (Nu) and coefficient of heat transfer (CHTC) behavior of AlO/water NFs in an automotive PFHE. Through this method, they optimized the NF concentration to achieve maximum performance; for CHTC, they measured up to a 56.3% increase in coefficient compared to the base fluid at an optimal 0.05% NP concentration that declined with higher concentrations due to the detrimental effect of both elevated viscosity and particle aggregation and measured the highest correlations to be an R of 0.9567 and R of 0.9762 in both models respective to Nu and CHTC. They then used an ANN and optimized heat exchanger volume with the same fluid in another investigation to maximize Nu and measured a considerable trade-off. Montazerifar et al. [16] investigated a three-stream PFHE with a fracture-type fin containing a different type of NF with computational fluid dynamics and optimization and measured a notable trade-off relationship between the three parameters: Nu, Colburn factor, and PP. Dhivagar et al. [17] took an experimental approach and showed that refrigerant distribution and load affected heat flux, CHTC, and effectiveness in a mini PFHE application for battery thermal management. Li et al. [18] employed four ML models to predict local CHTC and unit pressure drop of supercritical methane in a printed-circuit heat exchanger. The training data consisted of 6213 local data segments, and an ANN prediction for CHTC had an R value of 0.9994, while the pressure-drop prediction had an R value of 0.9996. When a trained ANN model was integrated into a 1D calculation, the results for T and pressure distributions agreed well with the numerical solution. Alharthi et al. [19] designed a feedforward ANN based on the Levenberg-Marquardt (LM) algorithm to predict Nu and the friction factor of AlO/water NF with conically coiled tubes. The correlation coefficient between predicted values and the test data was 0.9952 for Nu and 0.9482 for the friction factor, indicating that the LM training algorithm can well mimic nonlinear thermo-hydraulic behavior under limited-data conditions. For plate heat exchangers, Alklaibi et al. [20] experimentally analyzed FeO-SiO/water HNFs and proposed correlations and an ANN model for Nu, friction factor, and thermal performance. An optimized ANN gave an R^2 value of 0.965, and the proposed correlations predicted Nu with 2% error and the friction factor with 3% error. Borode et al. [21] used experiments, RSM, and ANN models to correlate thermal conductivity, electrical conductivity, and viscosity of GNP-FeO HNFs; the ANN models predicted these responses more accurately than RSM; however, it showed that an optimal number of hidden neurons is particular for each response-an ANN architecture suitable for prediction of a certain response might not applicable to prediction of other response. Aksöz et al. [22] used the ML in order not only to predict response but also to understand which variables, namely Re and geometry characteristics of vortex generator, cause changes in thermal performance indicator, Nu and friction factor using decision tree and eXplainable ML.

Table 1 summarizes the scope of the reviewed investigations and clarifies their relationship to the present study.

Three areas still need improvement. First, most reported models predicted thermophysical properties or a few heat-exchanger responses, such as Nu, CHTC, or friction factor. The coordinated evaluation of HT enhancement and circulation energy expenditure was less common. The second area relates to the databases used: although most ANN investigations used the thermophysical properties of either water-based NFs or traditional coolants, and artificial databases derived from computation, far less was published on transformer-oil-based mono & hybrid NFs in PFHEs in a data-driven way. Finally, high reported correlations derived from just one data split did not indicate model stability

Table 1
Comparison of previous studies and the present work.

Reference	Investigated system and method	Main outputs	Scope relative to the present study
Tekir et al. [12]	Fe_3O_4/water and Fe_3O_4–Cu/water HNFs in a plate heat exchanger; experimental	Effectiveness, Nu, CHTC	Examined coupled thermal responses but did not establish a multi-response surrogate framework
Patel et al. [13]	Cu and Al_2O_3 mono and hybrid NFs in a solar still; experimental	Productivity, efficiency	Demonstrated the importance of NP mixing ratio but did not examine PFHE thermal-hydraulic responses
Babaelahi et al. [14]	Plate-tube and fin heat exchangers; multi-objective optimization	Heat-exchanger volume, PP	Optimized thermal and hydraulic performance without developing a predictive ANN framework
Aktas et al. [15]	Al_2O_3/water NF in an automotive PFHE; experimental, ANN, and PINN	Nu, CHTC	Compared two learning approaches but focused primarily on thermal outputs
Montazerifar et al. [16]	Three-stream PFHE with an oil-based NF and fractal fins; numerical optimization	Nu, Colburn factor, PP	Investigated thermal-hydraulic optimization but not transformer-oil mono and hybrid NF prediction
Dhivagar et al. [17]	PFHE for battery thermal management; experimental	CHTC, heat flux, effectiveness	Examined compact heat-exchanger performance without data-driven prediction
Li et al. [18]	Supercritical-methane printed-circuit heat exchanger; numerical data and four ML models	Local CHTC, unit pressure drop	Provided ML validation but did not examine NFs or transformer-oil systems
Alharthi et al. [19]	Al_2O_3/water NF in conically coiled tubes; experimental and ANN	Nu, friction factor	Applied LM training but did not investigate a PFHE or hybrid formulation
Alklaibi et al. [20]	Fe_3O_4–SiO_2/water HNF in a plate heat exchanger; experimental and ANN	Nu, friction factor, thermal performance	Investigated an HNF but was limited to a water-based working fluid and fewer responses
Borode et al. [21]	GNP–Fe_2O_3 HNF; experimental, ANN, and RSM	Thermal conductivity, electrical conductivity, viscosity	Predicted fluid properties rather than system-level PFHE responses
Aksöz et al. [22]	Heat exchanger with vortex generators; ML and explainable analysis	Nu, friction factor, thermal performance indicator	Focused on geometric effects rather than NF formulation
Present study	MgO/transformer oil and MgO–CuO/transformer oil NFs in a PFHE; four independent ANN models	UHTC, CHTC, Re, PP	Integrates thermal and hydraulic predictions, compares mono and hybrid formulations, and evaluates model stability through repeated and cross-validated analyses

or generalizability: re-training independently with enough cross-validation runs, reporting errors with uncertainty analysis, and comparing different learning techniques had to be practiced, especially when the data was small and interpolated as described here.

1.3. Proposed framework, novelty, and paper organization

The current study aimed to determine whether the T and NF structure constitute an input space with sufficient information to predict UHTC, CHTC, Re, and PP for mono- and hybrid transformer oil NFs in the experimental range, enabling stable predictions. In response to the question, the experimental data on MgO/transformer oil and MgO-CuO/transformer oil NFs in PFHE, provided in reference Sandhya et al. [23] was first reproduced and consolidated into a continuous in-domain dataset, with T and NF structure (representing mono or hybrid formulation) as the inputs. Four separate feedforward ANN models, each trained to predict a single output using the LM algorithm (assuming the models were interpolative surrogate models rather than mechanistic flow models/extrapolation tools), were then developed. This study proposed three novel contributions to the current body of knowledge in this area. First, it proposes a consolidated architecture that incorporates four independent ANN models with two thermal response characteristics (UHTC, CHTC) and two hydraulic flow characteristics (Re, PP), providing insight into both the thermal benefit and the hydraulic cost of running with NFs within a single context. Second, it directly contrasted monotype NFs (MgO/transformer oil) with hybrid NFs (MgO-CuO/-transformer oil) under identical operating parameters and assessed how T and formulation influenced the predicted response sensitivities. Finally, it investigated the reliability of predictions through successive multiple independent training runs and statistics from 10-fold cross-validation and uncertainty calculations, as well as comparisons with commonly used other ML methods including support vector regression (SVR), random forest regression (RF), and a multilayer perceptron (MLP) trained with stochastic gradient descent (SGD). These additions demonstrated predictive stability versus agreement due to a favorable single partition.

2. Data reconstruction and ANN modeling methodology

2.1. Source data digitization and PCHIP reconstruction

Dataset: The dataset used in this study was reconstructed from the experimental thermo-hydraulic data as shown in the published figures by Sandhya et al. [23] corresponding to MgO/Transformer Oil and MgO-CuO/Transformer Oil NFs traversing the plate-fin heat exchanger. The WebPlotDigitizer tool [24] was used to digitize the numerical data for UHTC, CHTC, Re, and PP from the published figures. The available experimental responses were given at five nominal Ts of 30 C, 40 C, 50 C, 60 C, and 70^0 C. For each NF composition, the closest available digitized experiment to each nominal T was taken as a reference anchor. Some deviations were expected between the digitized and nominal values due to the figures' resolution and cursor position during data digitization. Nevertheless, the nearest nominal T was assigned to each anchor, enabling their usage in the later reconstruction procedure. A total of ten data points, comprising five operating Ts and two different composition NFs, were considered as the digitized reference anchors. A range of Ts from 30 C to 70^0 C with an interval of 1^0 C was designated, and a universal T grid (2.65, 2.65 + 1, …, 70) was created. Piecewise Cubic Hermite Interpolating Polynomial (PCHIP) [25] interpolation method, as implemented in MATLAB(®), was employed for each target response for each NF separately. Conventional cubic-spline interpolation was bypassed in favor of PCHIP for its ability to preserve the local shape and monotonicity of the digitized figures while avoiding non-physical overshooting between adjacent reference points. We obtained 41 T points for each NF composition, for a total of 82 points. Among these points, 10 corresponded to the digitized reference anchors (5 for each NF), whereas the remaining 72 were generated via interpolation and were not considered separate, statistically independent, or new experiments. Therefore, the developed model was interpreted as a data-driven surrogate model aimed at interpolating between the available operating conditions (T and NF composition). Two variables were used as ANN inputs; T was used as a continuously varying input, while NF composition type was used as a discrete, categorical input represented by the values 0 and 1 to describe MgO/Transformer Oil and MgO-CuO/Transformer Oil NF, respectively. The resulting models predict UHTC, CHTC, Re, and PP for either fluid mixture or either heat exchanger configuration under the considered Ts and NF compositions.

2.2. ANN architecture and training configuration

Four separate feedforward MLP networks were constructed to predict UHTC, CHTC, Re, and PP. The networks included two neurons representing T and NF structure as inputs, one hidden layer of five neurons, and one output neuron that predicted the target responses. So, a 2–5–1 MLP architecture was trained randomly and independently for each thermo-hydraulic property [24–26]. Separate single-output networks were used to avoid interaction among the target variables because of differences in response scales and behavior [27]. The tangent-sigmoid transfer function was used for the hidden layer to map the nonlinear input-to-output relationship, while the linear transfer function was applied in the output layer to obtain continuous predicted responses. The networks were generated in MATLAB R2018b using the Neural Network Toolbox and trained with the LM backpropagation algorithm. The maximum number of training epochs was set to 200, the normalized MSE goal was set to $1 \times 10\ -6$, and training stopped when validation performance did not decrease for six consecutive epochs. For each experiment, we selected the best model based on validation performance, without considering test performance.

2.3. Data preprocessing and repeated internal assessment

For every independent run, the reconstructed dataset was divided into training, validation, and test subsets using stratified random sampling based on NF structure. The proportions assigned to training, validation, and testing were 60%, 20%, and 20%, respectively. Because the reconstructed dataset contained 41 records for each NF formulation, each run contained 50 training records, 16 validation records, and 16 test records. Stratification ensured that both NF formulations were represented at comparable proportions in all three subsets. The training subset was used to determine the network weights and biases, while the validation subset controlled early stopping and model selection. The test subset was not involved in parameter estimation or model selection and was used only to evaluate internal reconstruction consistency. The minimum and maximum values required for input and output normalization were calculated exclusively from the training subset. We then applied these unchanged normalization parameters to the validation and test subsets, preventing information from the evaluation subsets from influencing preprocessing. To account for the sensitivity of ANN training to data partitioning and initial weights, we independently trained each of the four networks 30 times using distinct reproducible random seeds. We calculated performance indices separately for each run and reported the mean and standard deviation. Because the randomly divided records originated from the same reconstructed curves, we interpreted this assessment as an evaluation of ANN fitting stability and internal prediction consistency rather than independent experimental generalization.

2.4. Leakage-aware grouped anchor-holdout validation

A second validation approach was added to reduce the information leakage introduced by adjacent PCHIP records. The five nominal Ts were separated into distinct T classes. Within each of the five folds, all digitized anchors belonging to one nominal T were simultaneously deleted from each of the NF formulas before the PCHIP reconstruction. This ensures that the response values of the deleted anchor could not affect the reconstructed grid on which training was performed. A 2°C T buffer on either side of the deleted anchor T was also removed from the reconstructed training grid, limiting the influence of more recently interpolated data and imposing a tougher evaluation of the learned relationship. The remaining records were split into training (80%) and validation (20%) sets, and normalization parameters were computed solely on the training subset. The reconstructed anchors at 40, 50, and 600 °C were considered for interpolation, as they still fell within the interpolation boundaries created by the chosen reference anchors. However, the anchors at 30 and 70 °C' representing extrapolated boundary tests, were considered separately, as their removal resulted in training ranges of 40–70°C and 30–60°C' respectively. Thus, boundary behavior was not deemed reliable evidence of applicability beyond the experimental range of original data. Each grouped validation fold was repeated 30 times with different random initializations of the network; all held-out anchors had their predictions recorded and summarized as interpolation or extrapolation behavior (or all included), respectively. This anchor-level test was considered to be the primary test of prediction ability. Standard random 10-fold cross-validation across the 82 reconstructed records was avoided, as random sampling would significantly duplicate both original and derived (PCHIP-generated) points between training and testing folds, overstating generalization performance. This classification by nominal T was believed to represent a more conservative approach for a dataset of this type.

3. The LM training formulation

The weights and biases of each MLP were estimated using the LM algorithm, an efficient nonlinear least-squares optimization method for small and moderate-sized regression networks [28,29]. For the ith training sample, let y_i denote the reference response, $\hat{y}_i(w)$ the network prediction, and $e_i(w) = y_i - \hat{y}_i(w)$ the prediction error, where w is the vector containing all trainable weights and biases. The objective function minimized during training is

$$F(w) = \frac{1}{2}\sum_{i=1}^{m} e_i(w)^2 \tag{1}$$

For m training samples and p adjustable parameters, the Jacobian matrix contains the first derivatives of the residual vector with respect to the network parameters:

$$J_{ij} = \frac{\partial e_i(w)}{\partial w_j}, i = 1, \ldots, m; j = 1, \ldots, p \tag{2}$$

At iteration k, the gradient of the half-sum-of-squares objective and the Gauss–Newton approximation to its Hessian are given by Eqs. (3) and (4), respectively:

$$g_k = J_k^T e_k \tag{3}$$

$$H_k \approx J_k^T J_k \tag{4}$$

The LM update augments the Gauss–Newton matrix with a damping term and updates the parameter vector according to

$$w_{k+1} = w_k - \left(J_k^T J_k + \lambda_k I\right)^{-1} J_k^T e_k \tag{5}$$

Here, e_k and J_k are the residual vector and its Jacobian at iteration k, H_k is the approximate Hessian, I is the identity matrix, and $\lambda_k > 0$ is the damping factor. A relatively large λ_k produces small gradient-descent-like steps and improves robustness away from the minimum, whereas reducing λ_k makes the update approach the faster Gauss–Newton step near the solution [30]. The damping term also improves the numerical conditioning of the matrix in Eq. (5). These relations describe ANN parameter optimization; they do not govern fluid flow or HT.

3.1. Statistical performance measures

Prediction error was quantified using the mean squared error (MSE), root mean squared error (RMSE), mean absolute error (MAE), and mean absolute percentage error (MAPE). Agreement between the reference and predicted responses was assessed using the Pearson correlation coefficient (R) and the coefficient of determination (R^2) [31–34]. For n evaluation samples, these measures are defined as follows:

$$\mathrm{MSE} = \frac{\sum_{i=1}^{n}(y_i - \hat{y}_i)^2}{n} \tag{6}$$

$$\mathrm{RMSE} = \sqrt{\frac{\sum_{i=1}^{n}(y_i - \hat{y}_i)^2}{n}} \tag{7}$$

$$\mathrm{MAE} = \frac{\sum_{i=1}^{n}|y_i - \hat{y}_i|}{n} \tag{8}$$

$$\mathrm{MAPE} = \frac{100}{n}\sum_{i=1}^{n}\left|\frac{y_i - \hat{y}_i}{y_i}\right| \tag{9}$$

$$\mathrm{R} = \frac{\sum_{i=1}^{n}(y_i - \bar{y})(\hat{y}_i - \bar{\hat{y}})}{\sqrt{\left(\sum_{i=1}^{n}(y_i - \bar{y})^2\right)\left(\sum_{i=1}^{n}(\hat{y}_i - \bar{\hat{y}})^2\right)}} \tag{10}$$

$$\mathrm{R}^2 = 1 - \frac{\sum_{i=1}^{n}(y_i - \hat{y}_i)^2}{\sum_{i=1}^{n}(y_i - \bar{y})^2} \tag{11}$$

In Eqs. (6)–(11), y_i and $\hat{y}_i$ are the reference and ANN-predicted values, respectively; $\bar{y}$ and the overbarred $\hat{y}$ denote their sample means; and n is the number of evaluated samples. MSE has squared output units, RMSE and MAE retain the unit of the predicted response, MAPE is expressed as a percentage, and R and R^2 are dimensionless. The Pearson coefficient ranges from −1 to 1, with values approaching 1 indicating strong positive linear agreement. We calculated each metric separately for every independent run and reported the final performance as the mean ± standard deviation over 30 runs. Because the reconstructed dataset contains interpolation-generated samples, we interpreted the random-split results as internal reconstruction consistency, whereas the grouped anchor-holdout results served as a more stringent robustness assessment.

4. Performance stability over independent runs

Table 2 shows the performance of the developed models with respect to data partitioning and network initialization, including the mean and standard deviation of RMSE over the training, validation, and test sets for each ANN, as well as the test-set MAPE and R^2. All four response variables have a MAPE below 0.12%, while the mean test-set R2 was above 0.9996 for all four response variables. The closeness between the training and testing set errors also suggested the models faithfully reconstructed the response surfaces across data splits, a consistent pattern hidden by the reported single-trial test-set result.

5. K-fold cross-validation

Fig. 2(a–d) presents fold-wise RMSE values obtained from conventional ten-fold cross-validation for UHTC, CHTC, Re, and PP. The mean RMSE for UHTC was 3.67 W/m²·K, with values ranging from 1.91 to 5.44 W/m²·K. CHTC produced a mean RMSE of 1.072 W/m²·K, with a

Table 2
Mean ± standard deviation of ANN performance over 30 independent runs.

Output	Training RMSE	Validation RMSE	Testing RMSE	Testing MAPE (%)	Testing R^2
UHTC	1.732 ± 1.066	2.041 ± 1.045	2.379 ± 1.355	0.1131 ± 0.0733	0.999919 ± 0.000131
CHTC	0.718 ± 1.954	0.596 ± 0.921	0.926 ± 1.913	0.0588 ± 0.1091	0.999641 ± 0.001572
Re	0.429 ± 0.193	0.578 ± 0.308	0.639 ± 0.398	0.0805 ± 0.0355	0.999988 ± 0.000016
PP	$1.687 \times 10^{-7} \pm 1.626 \times 10^{-7}$	$2.570 \times 10^{-7} \pm 1.912 \times 10^{-7}$	$2.842 \times 10^{-7} \pm 1.873 \times 10^{-7}$	0.0229 ± 0.0158	0.999981 ± 0.000029

The RMSE values are reported in $W/m^2 \cdot K$ for UHTC and CHTC, as dimensionless values for Re, and in W for PP.

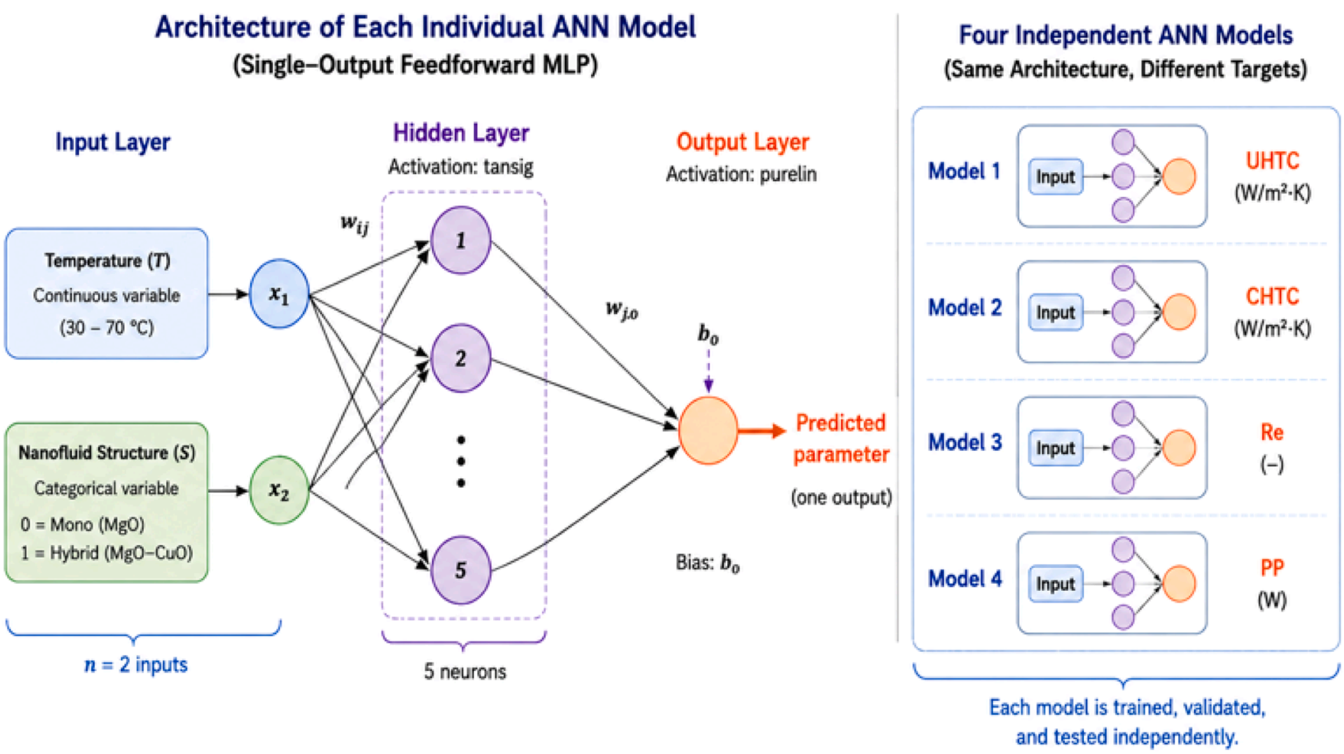

Fig. 1. Schematic representation of the single-output feedforward backpropagation neural network architecture independently developed for predicting UHTC, CHTC, Re, and PP.

range of 0.50–2.02 $W/m^2 \cdot K$. The corresponding mean RMSE for Re was 2.47, with minimum and maximum values of 1.62 and 3.17, respectively. For PP, the mean RMSE was 1.69×10^{-4} W, while the fold-specific values varied from 9.4×10^{-5} to 2.80×10^{-4} W. These results indicated that the response models did not exhibit the same degree of sensitivity to changes in fold composition. The relatively small errors for the two heat-transfer coefficients show that the networks reproduced the smooth T-dependent thermal responses in the reconstructed dataset. However, UHTC exhibited a broader fold-to-fold error range than CHTC. This difference relates to the physical meaning of these responses. CHTC primarily characterized convective exchange between flowing NF and the heat-transfer surface, whereas UHTC incorporated the combined effects of convective resistances, wall resistance, and the interaction between the thermal responses of heat-exchanger streams. UHTC therefore showed a more integrated system response and can exhibit stronger curvature when T and NF formulation are varied. The greater separation between the UHTC curves of mono and hybrid NFs, particularly at higher Ts, also made the prediction error more sensitive to which records were assigned to each fold.

In contrast, the comparatively gradual variation of CHTC provided a smoother relationship for the network to approximate. The narrow RMSE interval obtained for Re indicated that the model consistently reproduced the dominant monotonic variation of flow regime with T and NF structure. Physically, Re depended on the balance between inertial and viscous effects. Increasing T generally decreased the viscosity of transformer oil, thereby increasing Re under otherwise comparable flow conditions. Introducing MgO or MgO–CuO particles can additionally modify the effective viscosity and density, producing different Re responses for two NF formulations. Because the network was not supplied with viscosity and density independently, it did not explicitly calculate these mechanisms. Instead, T and NF structure acted as surrogate variables that encoded their combined influence within the experimental data. The limited fold-to-fold variation therefore indicated that this combined relationship was represented consistently, but it did not demonstrate independent learning of viscosity or density effects.PP displayed the largest relative variation among the fold-specific errors despite its small absolute RMSE. This behavior was physically reasonable because PP depended on pressure loss and volumetric flow rate and was consequently sensitive to relatively small changes in viscous resistance. T-induced viscosity reduction tended to decrease the pressure required to circulate the fluid, whereas NP addition may increase flow resistance depending on the resulting rheological properties. Small differences in the PP records assigned to each fold can therefore produce noticeable relative changes in RMSE because PP varied over a narrow numerical range. The absolute magnitude of its RMSE should therefore be interpreted alongside the scale of the response rather than considered alone. Overall, ten-fold results demonstrated stable fitting of the reconstructed response curves, particularly for UHTC, CHTC, and Re. Nevertheless, conventional random-fold cross-validation did not provide fully independent experimental validation in the present dataset.

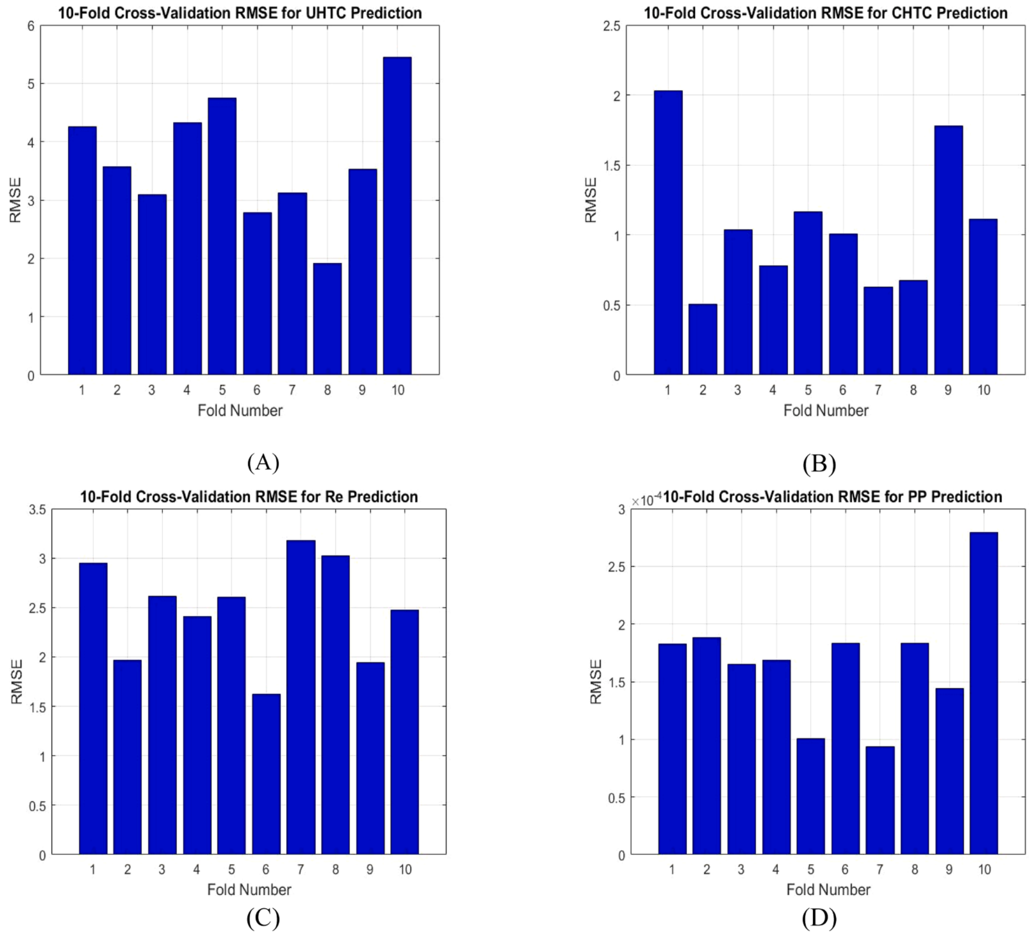

Fig. 2. Fold-wise RMSE values obtained from conventional ten-fold cross-validation for (a) UHTC, (b) CHTC, (c) Re, and (d) PP.

Neighboring PCHIP-generated records derived from the same experimental anchors may occur in both the training and test folds, allowing information from a common underlying curve to be represented in both subsets.

6. Prediction results and analysis

6.1. Comparing various performance functions

Fig. 3(a-d). Each converged to its validation best without oscillation or renewed error increase. For UHTC, CHTC, Re, and PP, the best validation epochs were 46, 18, 13, and 8, respectively. Such wide variance suggested that different amounts of parameter update were needed to characterize the input-output response of each measurement. As separate networks were trained for different-scale data, the relative MSE values were comparative only within each panel. The training, validation, and test errors for UHTC were 9.568, 5.015, and 11.018. The fact that the validation error was smaller than the training error did not mean the network was behaving abnormally; it merely indicated that randomly selected validation records happened to fall within a smoother range of responses.

The number of epochs required for the validation best for UHTC was the highest of the four, which made sense given that UHTC is a whole-system parameter and a summation/integration of multiple local contributions, like separated wall resistance and convective-wall resistance, not just one component like flow conditions at a single wall. As one increased T and/or NF formulation to make hybrid NF give an advantage over mono NF formulation (which was more efficient than separated wall T drop because it included HT along the wall in NF, not solely the resistance of wall HT and convective HT across the interface), UHTC curvature changed significantly as a result of the increased thermal merit of hybrid NF. It hence needed longer training and more parameter adjustments to capture those variable slopes for mono- and hybrid NF cases. The CHTC and Re reached their validation optima at epochs 18 and 13, respectively; their training/validation/test errors were 0.365/0.520/1.734 and 3.55/2.35/6.90, respectively. Note that the test error was generally larger than the others, as the selected test subset might have fallen within a more stringent operating-condition region than the training or Validation Sets. Also important, there was no indication that the training data fit the pattern better than the validation data for too long before early stopping occurred. CHTC was a measure of convective heat-transfer coefficient; Re measured the flow state. Both characteristics mostly depended on the combined effect of thermophysical properties, not the direct impact of T at a specific location or from one location, as other responses did. Thus, their T-dependent pattern tended to be more "monotonic," allowing faster convergence with fewer parameter adjustments to capture these relationships, while the NF formulation served only as a surrogate for different combinations of fluid mixtures under operating conditions.

The fastest-converging model, PP, reached optimal validation at epoch 8, and its training/validation/test MSE were 0.688/1.959/0.943, respectively. The increased validation error may suggest that PP was more sensitive to specific data records in its selected validation partition. Because PP is determined by energy and flow rate, variations in fluidity (viscosity) and the system's flow resistance may induce differences even at small flow rates or small P, or in small P drops. However, the PP response followed a simple relationship with T, so a relatively short epoch was required.

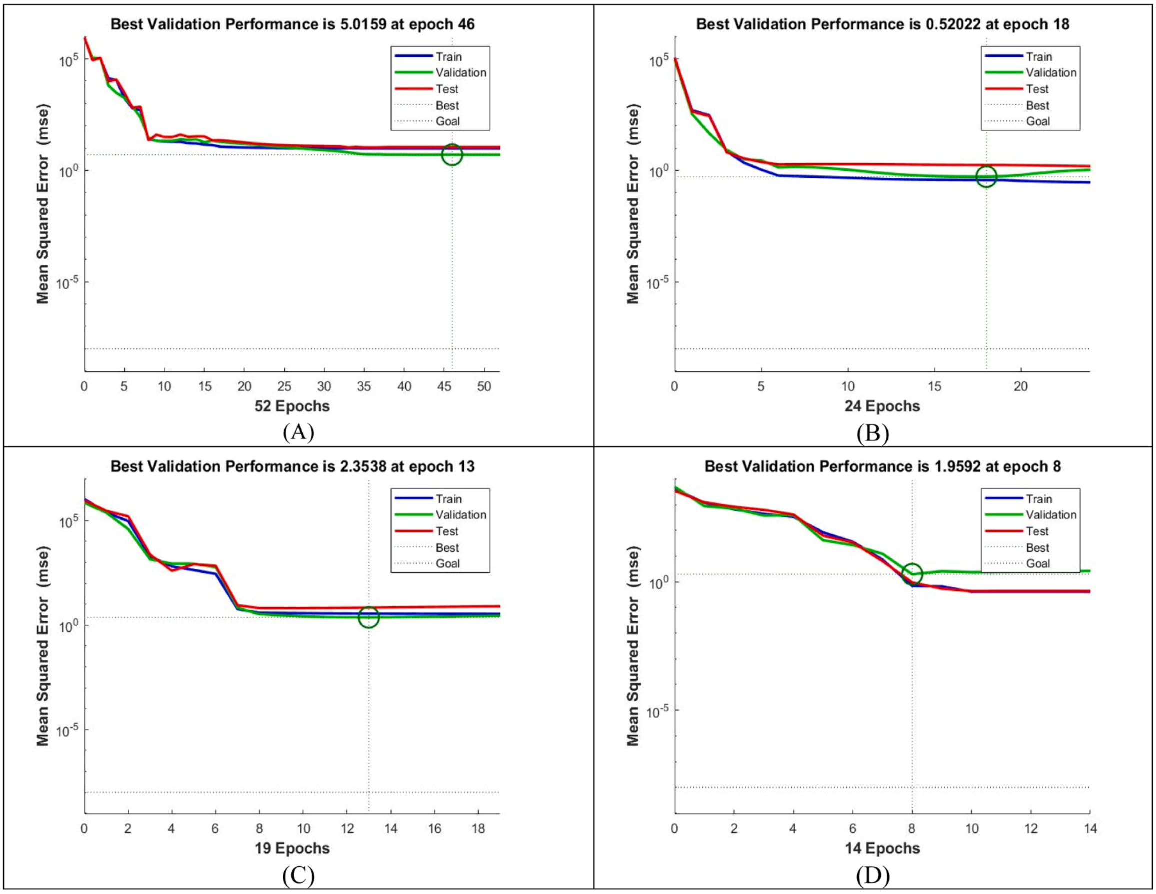

Fig. 3. Evolution of MSE during the training of the independently developed MLP–LM models for (a) UHTC, (b) CHTC, (c) Re, and (d) PP, showing the training, validation, and test subsets.

Fig. 4(a–d) compares the ANN-predicted values with the corresponding reference responses for UHTC, CHTC, Re, and PP. The training, validation, and test records were distinguished using different markers, while the identity line represented perfect agreement. For UHTC, the correlation coefficients were 0.99995, 0.99999, and 0.99996 for the training, validation, and test subsets, respectively, with an overall R of 0.99996. The corresponding values for CHTC were 0.99998, 0.99999, and 0.99993, resulting in an overall R of 0.99997. Reproduced R values of 0.99996, 0.99997, and 0.99993 and an overall value of 0.99996, whereas the PP model yielded 0.99995, 0.99980, and 0.99993 and an overall R of 0.99993. Thus, all four models preserved a strong linear correspondence between the predicted and reference values across the three data subsets. The thermal responses followed the identity line over the ranges represented by both NF formulations. For UHTC, the model reproduced not only the general increase with T but also the progressively greater separation between the mono- and hybrid-NF responses at higher Ts. This behavior indicated that the effect of NF formulation on UHTC was not represented as a constant offset; rather, its contribution varied across the investigated T range. Such behavior is consistent with the system-level nature of UHTC, which incorporated changes in convective resistance and the overall heat-transfer pathway. CHTC exhibited less separation and a smoother variation, explaining the compact distribution of its predicted values around the identity line. T-dependent viscosity reduction can promote fluid motion and thermal-boundary-layer renewal, while NP dispersion modifies the fluid's effective thermal transport. However, because viscosity and thermal conductivity were not independent ANN inputs, the regression agreement reflects the combined experimental influence of these mechanisms rather than their separate quantitative contributions. The Re and PP results revealed an important coupling between flow enhancement and circulation-energy demand. Re increased with T, whereas PP generally decreased. These apparently opposite responses may originate from the same T-dependent mechanism: reduced transformer-oil viscosity increases the ratio of inertial to viscous forces and therefore raises Re, while simultaneously reducing flow resistance and the pressure loss contributing to PP. The NF formulation shifted both hydraulic responses because particle addition modified the effective density, viscosity, and internal flow resistance. The close alignment for Re indicates that the network consistently represented its strong monotonic T dependence. PP showed the largest reduction in validation correlation, from 0.99995 for training to 0.99980 for validation. Although this value remained high, the difference confirms that PP was more sensitive to the composition of the validation subset, consistent with the training-history results and its comparatively narrow response range.

Fig. 5(a–d) compares the reference and ANN-predicted values for the test subset and presents the corresponding absolute percentage error (APE) for each response. The UHTC predictions produced APE values between 0.0084% and 0.6566%, while the CHTC errors ranged from 0.0190% to 0.7593%. The corresponding ranges were 0.0171–0.7610% for Re and 0.0080–0.2914% for PP. Thus, the maximum pointwise error remained below 0.8% for all four responses in this particular random test partition. The predicted curves closely followed the reference profiles without persistent separation, indicating that the selected test subset contained no large systematic offset. The thermal models reproduced both the magnitude and T-dependent variation of UHTC and CHTC. The slightly wider error ranges observed for these quantities, compared with PP, can be related to differences in their response complexity.

UHTC represented the combined thermal resistance of the heat-exchanger system and exhibited a stronger distinction between the

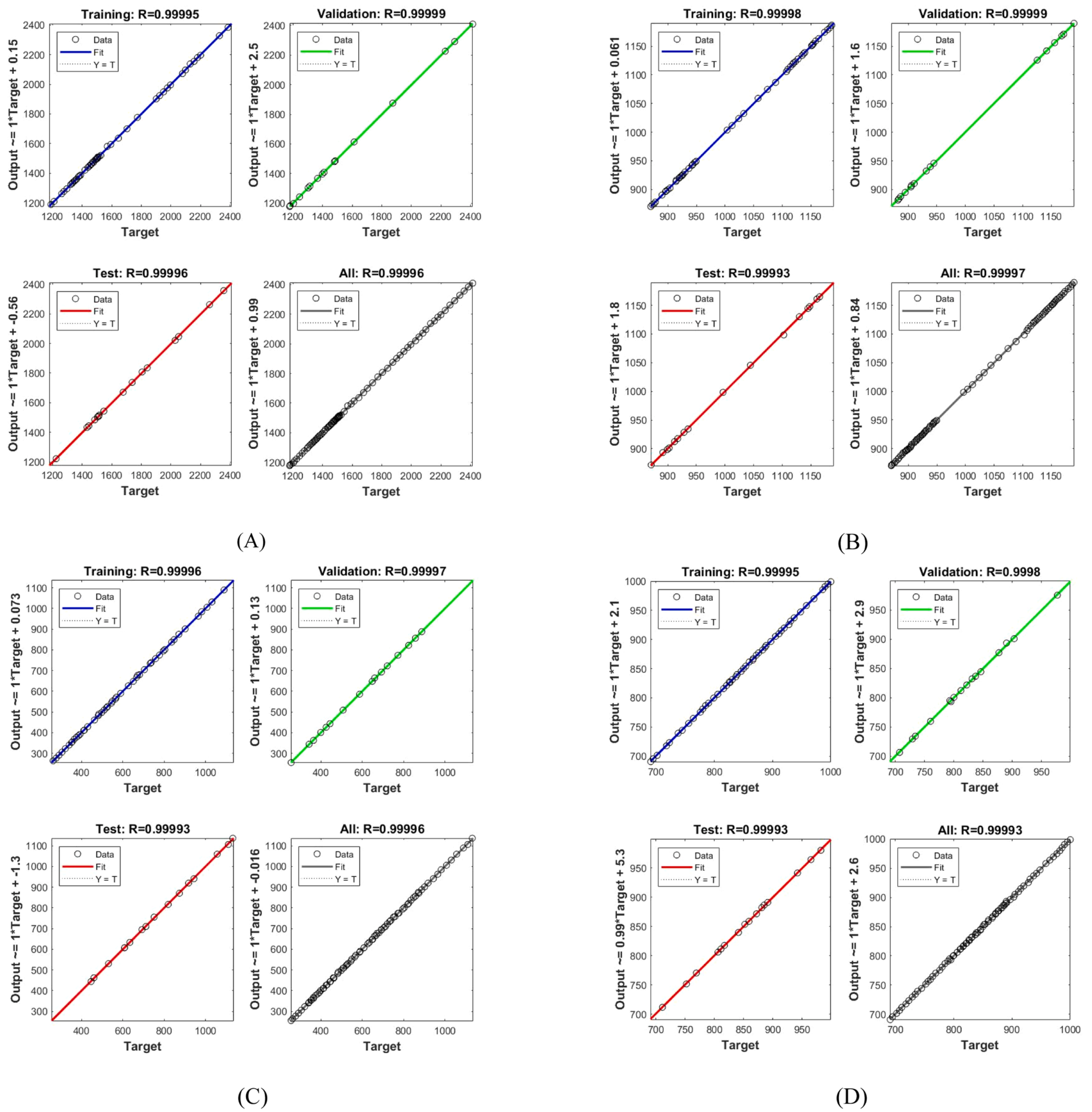

Fig. 4. Comparison between ANN-predicted and reference values for (a) UHTC, (b) CHTC, (c) Re, and (d) PP.

mono and hybrid NF formulations as T increased. CHTC was governed more locally by convective transport and thermal-boundary-layer behavior, but it remained sensitive to the coupled changes in viscosity, thermal conductivity, and fluid motion. Consequently, records located in regions where the thermal responses change more rapidly can be more difficult to approximate than those belonging to smoother portions of the reconstructed curves. Nevertheless, the maximum APE values of 0.6566% and 0.7593% indicate close pointwise agreement for UHTC and CHTC, respectively. Re also showed close agreement between the predicted and reference values, although it produced the highest maximum APE (0.7610%). Re increased markedly with T because the reduction in transformer-oil viscosity increased the relative contribution of inertial forces. The NF formulation additionally shifted the Re response through its combined effects on density, viscosity, and flow behavior. These effects produced a comparatively broad response range and different slopes for the two NF formulations. The small pointwise deviations indicated that the network followed these variations within the test partition; however, they did not establish that viscosity and density were learned as independent physical quantities because neither parameter was supplied directly to the model.PP exhibited the narrowest APE interval, with a maximum value of 0.2914%. Its prediction curve followed the gradual reduction in circulation-energy requirement as T increased. This decrease was consistent with lower viscous resistance and pressure loss as the transformer oil became less viscous. At the same time, the hybrid NF maintained a different PP level because particle composition modified the effective hydraulic resistance. The

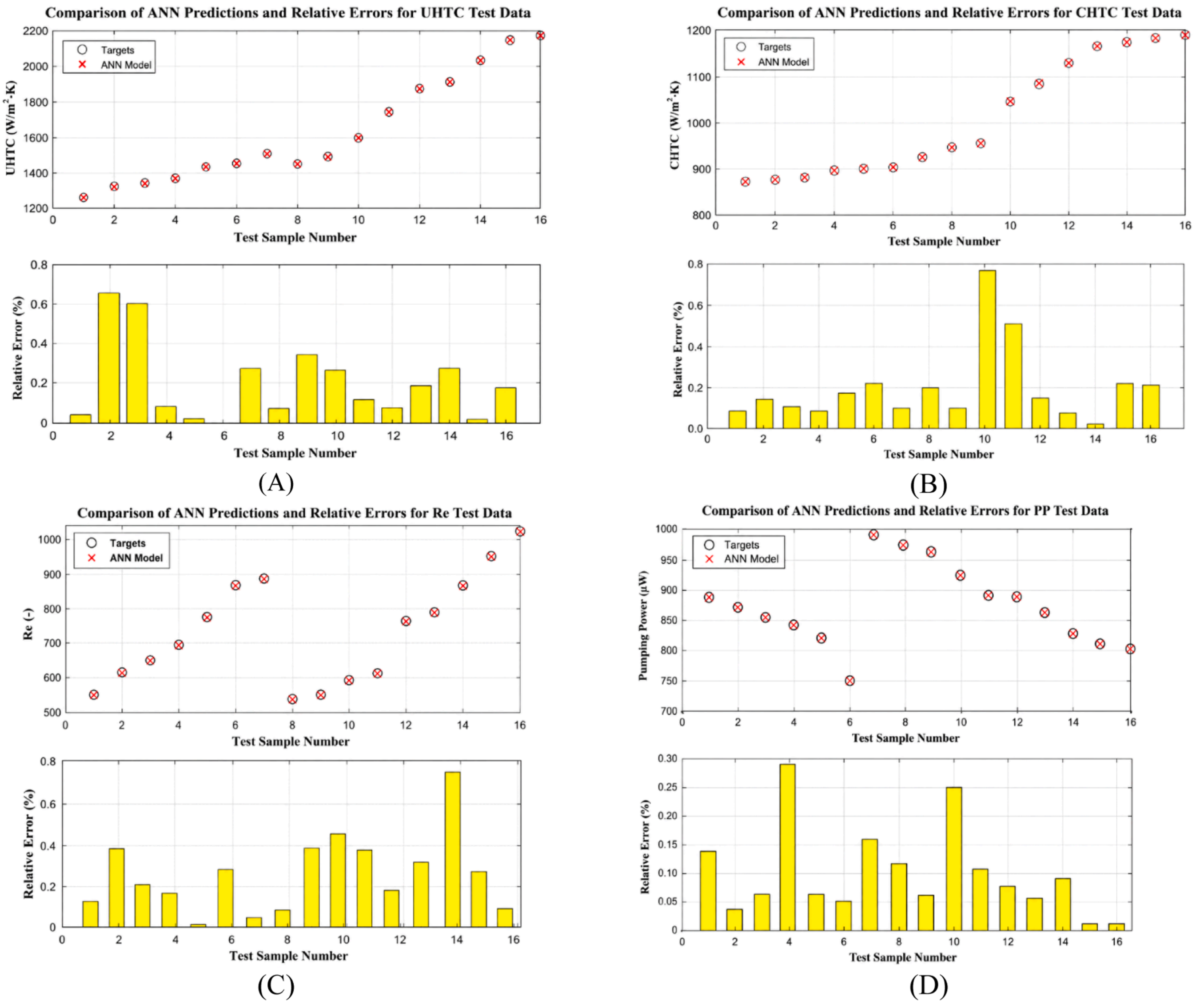

Fig. 5. Comparison between reference and ANN-predicted values and the corresponding absolute percentage errors for the test subset: (a) UHTC, (b) CHTC, (c) Re, and (d) PP.

smooth, monotonic character of these variations provided a more regular relationship for the ANN to approximate, resulting in smaller pointwise percentage errors than those obtained for the other responses.

6.2. Comparison with alternative machine-learning models

MLP-LM was trained on the same data, preprocessing, and anchor-holdout split setting as SVR-RBF, RF, and MLP-SGDM. MLP-SGDM used the same 2–5–1 architecture as MLP-LM to evaluate only the training-data process. Table 3 presents results with internal holdout Ts of 40, 50, and 60 °C, averaged over 30 independent experiments.

The ordering of models depended on the prediction variable, with MLP-SGDM being best for UHTC and PP; for the response Re, SVR-RBF performed best; the minimum mean RMSE for CHTC came from RF, but with a nearly 15-fold larger standard deviation for R than for MLP-LM and a much larger MAPE; the RF lower mean RMSE was therefore the best with considerably increased variability, with MLP-LM not being optimal for all responses, but for all cases still yielding good R-values (between 0.97838 and 0.99789) and MAPE-values (between 0.280% and 2.363%) with constant standard deviations of R less than 0.00074 over any single response. The errors increased when removing the holdouts at the boundary anchor points at 30 and 70 C. Considering all combined internal and boundary holdouts, MLP-LM gave the lowest error on CHTC and Re, and second on UHTC and PP. These results therefore establish MLP-LM as a balanced performer across the four responses, even if it is not optimal for every response, and with more limited capability for CHTC and Re than for UHTC and PP, with limitations related to model and dataset characteristics as stated above and analyzed further below. The results at boundary anchors, interpreted as stress tests, do not suggest any extrapolative capabilities beyond the presented range. Table 4 gives the performance of the MLP–LM models against held-out experimental anchors over 30 independent runs.

6.3. Validation against held-out experimental anchors

We assessed the predictive robustness of MLP-LM models on the digitized experimental anchors used in [23]. We withheld anchors recorded at one nominal T during each validation fold of both NF formulations during PCHIP reconstruction. Anchors recorded within ±2 °C of held-out T were not included in model creation. The anchors tested therefore had neither direct nor interpolating contributions to the models.

Table 3
Performance of the investigated models for internal grouped anchor holdout at 40, 50, and 60°C.

Output	Model	RMSE, mean ± SD	MAPE (%), mean ± SD	R^2, mean ± SD
UHTC	MLP–LM	42.994 ± 0.651	2.363 ± 0.043	0.97838 ± 0.00066
UHTC	SVR–RBF	43.468 ± 1.427	2.467 ± 0.107	0.97788 ± 0.00145
UHTC	RF	54.255 ± 9.719	2.557 ± 0.462	0.96451 ± 0.01138
UHTC	MLP–SGDM	38.408 ± 3.110	2.047 ± 0.218	0.98264 ± 0.00279
CHTC	MLP–LM	8.530 ± 0.218	0.433 ± 0.023	0.99424 ± 0.00029
CHTC	SVR–RBF	8.359 ± 0.139	0.449 ± 0.016	0.99447 ± 0.00019
CHTC	RF	7.966 ± 3.296	0.565 ± 0.143	0.99415 ± 0.00580
CHTC	MLP–SGDM	12.178 ± 0.608	0.767 ± 0.074	0.98825 ± 0.00116
Re	MLP–LM	7.780 ± 1.019	1.055 ± 0.106	0.99783 ± 0.00074
Re	SVR–RBF	6.011 ± 0.730	0.793 ± 0.108	0.99871 ± 0.00034
Re	RF	41.615 ± 6.020	6.563 ± 0.831	0.93773 ± 0.01860
Re	MLP–SGDM	15.815 ± 5.277	2.128 ± 0.576	0.99024 ± 0.00701
PP	MLP–LM	(3.015 ± 0.083) × 10^{-6}	0.280 ± 0.007	0.99789 ± 0.00011
PP	SVR–RBF	(3.517 ± 0.252) × 10^{-6}	0.364 ± 0.028	0.99711 ± 0.00041
PP	RF	(10.143 ± 1.764) × 10^{-6}	1.053 ± 0.223	0.97541 ± 0.00853
PP	MLP–SGDM	(2.634 ± 0.356) × 10^{-6}	0.263 ± 0.041	0.99836 ± 0.00044

Table 4
Performance of the MLP–LM models against held-out experimental anchors over 30 independent runs.

Output	Validation scope	RMSE, mean ± SD	MAPE (%), mean ± SD	R^2, mean ± SD
UHTC	Internal interpolation	42.994 ± 0.651	2.363 ± 0.043	0.97838 ± 0.00066
UHTC	Boundary stress test	125.243 ± 31.368	6.766 ± 1.839	0.92358 ± 0.04101
CHTC	Internal interpolation	8.530 ± 0.218	0.433 ± 0.023	0.99424 ± 0.00029
CHTC	Boundary stress test	38.874 ± 8.396	2.915 ± 0.668	0.88560 ± 0.05678
Re	Internal interpolation	7.780 ± 1.019	1.055 ± 0.106	0.99783 ± 0.00074
Re	Boundary stress test	32.687 ± 14.817	6.148 ± 3.426	0.99047 ± 0.01026
PP	Internal interpolation	(3.015 ± 0.083) × 10^{-6}	0.280 ± 0.007	0.99789 ± 0.00011
PP	Boundary stress test	(13.921 ± 4.058) × 10^{-6}	1.502 ± 0.396	0.98389 ± 0.00985

The RMSE units for UHTC and CHTC were W/m^2·K; Re was dimensionless, and PP was W. Internal interpolation was defined as having anchors at 40, 50, and 60 °C, while 30 and 70 °C were used as boundary stress tests. The MAPEs for the internal anchors were 2.363%, 0.433%, 1.055%, and 0.280% for UHTC, CHTC, Re, and PP, respectively, and R ranged from 0.97838 to 0.99789. These results show that the models recovered the experimental answers reported in the referenced experimental data at points outside the training sets, rather than merely replicating nearby anchor points from a PCHIP-generated curve database. Higher error in the case of UHTC is due to more nonlinearity in the dependence of this property (especially for hybrid NF) on T, in comparison with CHTC and PP. Holding out boundary points was predicted to increase the error because the prediction required extrapolation outside the restricted region where all anchors had been used. This was most visible for UHTC and Re, where the boundary MAPEs rose to 6.766% and 6.148%, respectively, whereas CHTC and PP remained insensitive, with MAPEs of 2.915% and 1.502%. When all ten held-out anchors were considered together, the MLP-LM models achieved MAPEs of 4.124% for UHTC, 1.426% for CHTC, 3.092% for Re, and 0.769% for PP. The distinction between internal and boundary errors delineates the conditions under which the models can be used effectively, i.e., to interpolate between the experimental points in the given range of Ts, but not to extrapolate beyond that range without further independent validation. Since all referenced anchors come from Digitized data from the original experiments used to build the base, validation here should not be considered for fully external models, but only as leakage-aware testing with unseen data from the same experiments.

6.4. *Shapes of fitted functions*

Fig. 6a-d show the absolute prediction error as a function of T for both the mono NF and hybrid NF on the total reconstructed dataset. Here, each of the four responses had different ranges and magnitudes in which the error peaked; therefore, the difficulty of prediction was not uniform over the domain of T or across the different NF formulations. As expected, the mono-NF error profiles were generally smoother, whereas the hybrid NF varied more locally. This behavior reflects, more than any direct interpretation of learning particle-scale interactions through the ANN, how much greater the degree of curvature, therefore the T dependency of these responses, was in the hybrid response versus the mono response. The range in the AE, when UHTC is the variable, was between 0.0429 and 31.883 W/m^2·K (mean 5.929 W/m^2·K, mean relative error 0.340%). The largest deviations were primarily limited to high-T regions of the hybrid NF, where the deviation increased as the UHTC rose rapidly and a larger gap opened between the mono- and hybrid responses. The ANN therefore had to approximate both the general response to varying T and the separation in each NF's response in T. Small peak errors indicated local regions of greater curvature where learning becomes less accurate, rather than errors throughout the NF. The error range for CHTC was 0.011–6.735 W/m^2·K (mean 1.529 W/m^2·K, mean relative error 0.147%), and deviations were primarily limited to the low T region in the hybrid NF. Transformer oil has higher viscosity at low Ts, which limits circulation of the working fluid and affects the T boundary layer and thus the prediction accuracy of CHTC, where even a small modification to effective thermo-hydraulic parameters can result in greater disparity in prediction of CHTC, where over this range and increases again in high T areas. This suggests there may be some form of loss when modeling high-T areas for CHTC, where the response appears flatter over a wider range as the solution passes smoothly over this portion of the data. Since viscosity and the T boundary layer were not included as inputs, the trend interpretations are physical rather than explanations of the learning process. For the PP variable, the AE ranged from roughly 0.0286 10–2.246 10 W (mean 0.587 10 W). Deviations tended to be mostly confined to the low T portions of the hybrid NF which suggests they are due to the correlation between PP and viscosity in that even small differences the thermo-hydraulic properties will lead to differences in the predicted value with this variable since viscosity can be varied extensively as the function is modeled across the varying Ts (as mentioned before, the resistance to fluid flow at low Ts can be quite a bit greater than at high T as viscosity decreases). This again explains why the error is the way it is, rather than what the network learned specifically.

6.5. *Engineering applications*

This ANN-based approach for design, operation, and design

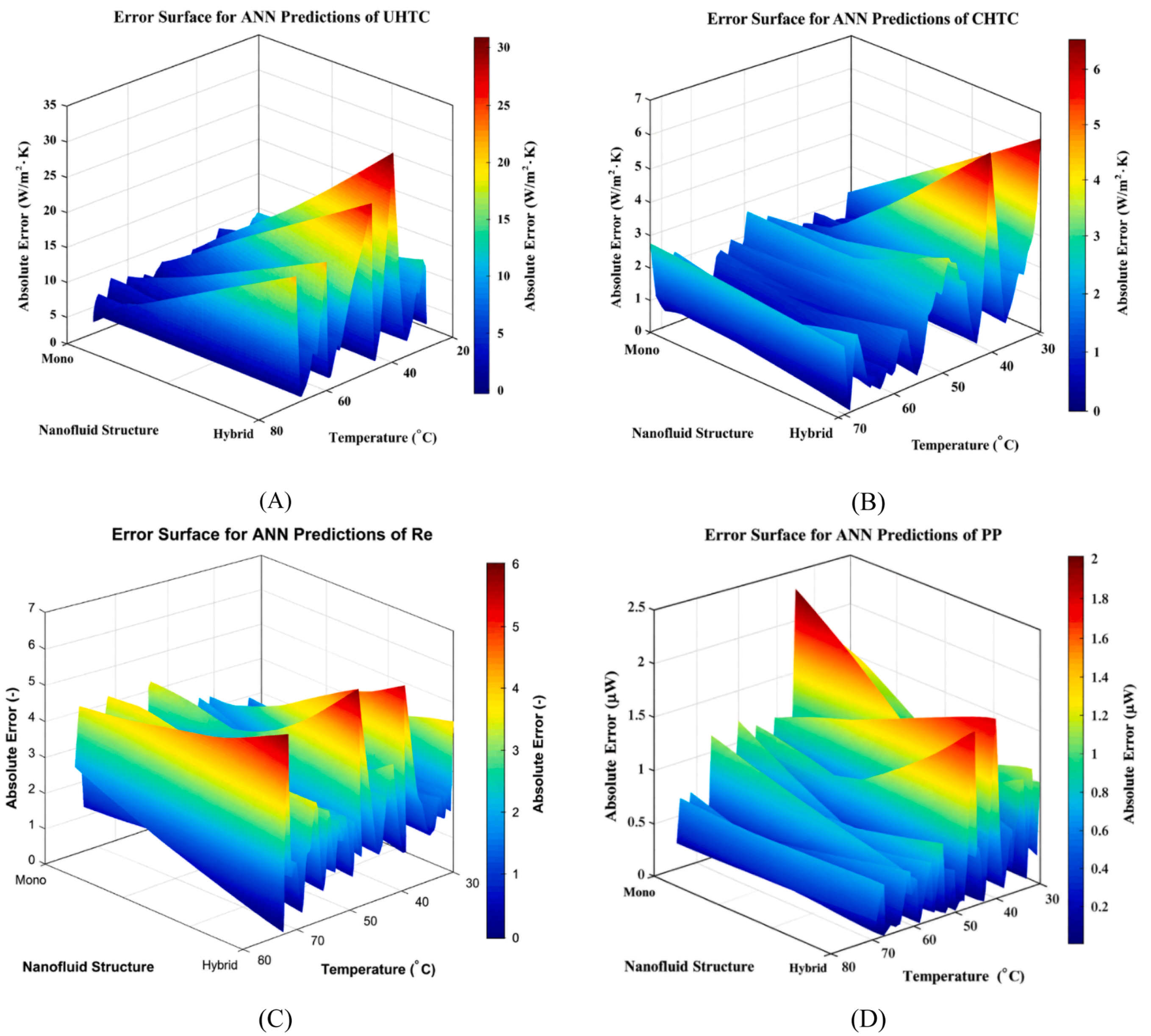

Fig. 6. Variation of absolute prediction error with T for the MgO/Transformer Oil and MgO–CuO/Transformer Oil NFs: (a) UHTC, (b) CHTC, (c) Re, and (d) PP.

optimization was applied to NF-based plate-fin heat exchangers under varying operating conditions. Thermo-hydraulic performance parameters of such exchangers are difficult to obtain experimentally or numerically in typical engineering practice, which requires significant time and computational resources. This study provides an alternative for quickly predicting UHTC, CHTC, Re, and PP from operating T and NF structure, saving engineers significant time in the preliminary design and functional analysis stage. From a design perspective, the proposed method helps determine operating conditions for best performance and lowest fluid-flow expenditure, as it predicts both thermal and hydraulic parameters at once; functional balance can then be evaluated easily without additional experiments compared with conventional engineering design. This method is especially powerful for small, compact thermal systems, where small changes in conditions can lead to large fluctuations in overall efficiency. In addition, the proposed method is also valid for transformer oil, especially with NP-doped transformer oil NFs, which can improve heat dissipation in the transformer; it is useful to determine which option offers good cooling performance by estimating it through simulation before experimental work for such a study.

Furthermore, it is a useful tool for predicting and selecting a suitable NF recipe. Moreover, this ANN-based method is not limited to oil cooling of transformers; it may also be used in digital environments, optimization algorithms, and real-time monitoring as a surrogate model. Training requires negligible resources, so engineers can carry out design and optimization effectively on these factors.

7. Variance-based sensitivity analysis

A Variance-Based Sensitivity Analysis was conducted to evaluate the contribution of T-related uncertainties in the total variation of ANN-predicted thermo-hydraulic performance. Since the structure of the NF was a discrete variable that had two states (MgO/Transformer Oil and MgO-CuO/Transformer Oil) and therefore could not be entered as a continuous parameter into the calculation of variance of input contribution, its impact was evaluated by directly comparing the performance of two selected MW-CTs over the same ranges of input variables. The ANN surrogate models were then used to estimate the evolution of UHTC, CHTC, Re, and PP as a function of T variation over the considered

T range (30 C to 70 C), while keeping the NF structure constant for each case under study. Table 5 summarizes the T sensitivity indices for the selected NFs. A variation in the sensitivity of T to different thermo-hydraulic parameters, as well as to the type of MW-CT, was observed. For the MgO/Transformer Oil MW-CT, T had the least influence on the HT-related variables, with relative contributions of 0.085 and 0.037 to UHTC and CHTC variations, respectively. Because Re and PP are related to flow-related variables, T showed relatively greater sensitivities of 0.641 and 0.527, respectively, due to the greater dependence of flow parameters on T, which dictates the competition between inertial and viscous forces. In the case of MgO-CuO/Transformer Oil-HNFs, T played a far greater role in the thermo-hydraulic performance of the MW-CT. T's impact on the HT-related quantities UHTC and CHTC was rather large (0.759 and 0.177, respectively); thus, a stronger interdependence between the changes in T and thermal characteristics was realized in the case of MW-CT with enhanced HNFs. Furthermore, T was found to be extremely effective in describing the predicted flow characteristics of MW-CT with MgO-CuO/Transformer Oil-HNFs: its contribution to variation in Re was as high as 1.000, making T the leading variable in determining the prediction of the flow behavior, whereas its sensitivity with PP was considerable (0.543).

The outputs showed that parameter T was the main determinant of the hydraulic properties of the considered NFs, while the dependence of HT properties on T was strongly modulated by NF composition. The higher sensitivity of MgO-CuO/Transformer Oil NF suggests that integrating hybrid NPs changed the T-dependent thermo-hydraulic response of the base fluid. To evaluate the contribution of NF structure, we compared two different NF recipes rather than continuously varying the nominal input variables.

8. Conclusion

In this study, we developed four independent single-output MLP–LM models to estimate UHTC, CHTC, Re, and PP for MgO/Transformer Oil and MgO–CuO/Transformer Oil NFs in a plate-fin heat exchanger. T and NF structure were used as the governing inputs. The models were evaluated through repeated independent runs, cross-validation, internal and boundary holdout tests, and comparison with SVR–RBF, RF, and MLP–SGDM. Accordingly, model reliability was assessed using error-based criteria and variability across independent runs rather than relying solely on Rs. The principal findings are summarized as follows:

- The developed MLP–LM models accurately represented the nonlinear relationships between the selected inputs and the four thermo-hydraulic responses within the investigated operating domain.
- In the repeated internal-holdout evaluation, the mean MAPE values of MLP–LM were 2.363% for UHTC, 0.433% for CHTC, 1.055% for Re, and 0.280% for PP.
- The corresponding mean R^2 values ranged from 0.97838 for UHTC to 0.99789 for PP, confirming strong in-domain agreement between the predicted and reference values.
- The relatively small standard deviations obtained over 30 independent runs indicated that the MLP–LM results were not strongly dependent on a particular network initialization or random data partition.
- The comparison showed that no learning algorithm achieved the lowest prediction error for all four outputs. Model performance was therefore dependent on the response being predicted.
- MLP–SGDM produced the lowest internal-holdout RMSE for UHTC and PP, with values of 38.408 $W/m^2{\cdot}K$ and 2.634×10^{-6} W, respectively.
- SVR–RBF achieved the lowest RMSE for Re (6.011), while maintaining an R^2 of 0.99871.
- RF produced the lowest mean CHTC RMSE of 7.966 $W/m^2{\cdot}K$. However, its standard deviation of 3.296 $W/m^2{\cdot}K$ and higher MAPE revealed greater sensitivity to data partitioning and bootstrap sampling.
- Although MLP–LM was not individually superior for every response, it provided consistently low errors and limited run-to-run variability across all four outputs. This balanced behavior supported its selection as the principal surrogate model.
- The boundary-holdout assessment was more demanding than the internal evaluation and produced higher prediction errors, particularly near sparsely represented T boundaries.
- When all internal and boundary anchors were considered, MLP–LM achieved the lowest RMSE for CHTC and Re, with values of 25.491 $W/m^2{\cdot}K$ and 21.653, respectively.
- MLP–SGDM achieved the lowest boundary-holdout RMSE for UHTC and PP, while MLP–LM ranked second for both responses. RF exhibited the greatest deterioration near the domain boundaries.
- The difference between internal and boundary-holdout results demonstrated that very high internal correlation values alone are insufficient to establish model generalization.
- The sensitivity analysis indicated that the influence of T was dependent on NF formulation. The hydraulic responses, particularly Re and PP, showed greater T sensitivity for the MgO–CuO/Transformer Oil HNF.
- Physically, increasing T changes the viscosity and density of transformer oil and consequently modifies the balance between inertial and viscous forces. These changes directly influence Re, flow resistance, and the PP required for fluid circulation.
- NF structure altered the thermal and hydraulic responses by modifying the effective heat-transfer pathways and flow resistance. Therefore, the thermal advantage of the HNF should be evaluated together with its associated hydraulic demand.
- The developed models provide rapid estimates of UHTC, CHTC, Re, and PP and can support preliminary screening of operating conditions for the investigated plate-fin heat exchanger.
- The framework's practical applicability is restricted to MgO/Transformer Oil and MgO–CuO/Transformer Oil NFs within the studied T range. The models should not be used for unrestricted extrapolation or as substitutes for independent experiments.

Table 5
The sensitivity indices that obtained from the variance-based sensitivity analysis.

NF	UHTC	CHTC	Re	PP
MgO/Transformer Oil	0.085	0.037	0.641	0.527
MgO–CuO/Transformer Oil	0.759	0.177	1.000	0.543

8.1. Limitations and future work

The form and size of the database used largely limit the applicability of the presented models. The numerical points were digitized from published experimental curves via WebPlotDigitizer and interpolated via PCHIP interpolation, which maintained the depicted trends and excluded unphysical oscillations in neighboring data points; however, the interpolated points still depend mathematically on the original digitized points and do not truly represent a new experimental measurement. The smoothing effect of interpolation likely contributes to the surprisingly accurate performance for the randomly held-out interior divisions. In this case, successive rounds of regrouped anchor-holdout and boundary-holdout evaluations somewhat diluted the trend of high performance. This approach still cannot substitute for true validation on new, raw experimental data, however. Further limits on the predictive region include the single plate-fin heat-exchanger geometry, the two different transformer oil NFs, and the T range of 30–70°C employed. Accordingly, T and NF composition served as aggregate parameters that represent many physical effects not independently measured. Thus, they do not capture the individual impact of viscosity, density, thermal conductivity, nanoparticle (NP) volume fraction, particle size, mass flow rate, or pressure drop. The neural networks predict their combined effect, but cannot attribute effects individually or claim causality. So, as they currently exist, the models are best viewed as in-domain predictors rather than models that will necessarily accurately depict the flow, the boundary layer, or the viscous resistance. The framework could be generalized through increased experimentation across different T ranges, mass flow rate ranges, and more Nf's with wide and varied variations in np concentrations and np size, along with other heat exchanger geometries, to better understand and utilize heat exchangers that operate in various scenarios. Adding these and other thermophysical parameters directly into model inputs could lead to more meaningful and interpretable predictions, and the error analysis should incorporate and express intervals on model predictions, since they are near domain boundaries. With physics-based constraints enforced, the connection to fundamental thermo-hydraulic concepts may be strengthened in future work, as the current approach primarily relies on implicit inference. Then, upon validation through diverse experiments, the resulting framework could be coupled with Multi-objective Optimizations aimed at manipulating those conditions to improve both UHTC and CHTC while keeping PP at a minimal level.

CRediT authorship contribution statement

Narinderjit Singh Sawaran Singh: Methodology, Investigation, Funding acquisition, Formal analysis, Data curation, Conceptualization, Writing – original draft, Writing – review and editing, Software, Validation. **Abdalmalik N. Attallah:** Methodology, Investigation, Funding acquisition, Formal analysis, Data curation, Conceptualization. **Muntadher Abed Hussein:** Methodology, Investigation. **Mithaq Nazar Jassim:** Writing – original draft; Writing – review and editing, Software, Validation. **Ahmed Najat Ahmed:** Software, Validation. **Hakim AL Garalleh:** Methodology, Investigation, Funding acquisition. **Zuhair Jastaneyah:** Methodology, Investigation, Writing – original draft, Writing – review and editing, Software, Validation. **Mahmut Taner:** Conceptualization, Writing – original draft, Writing – review and editing, Software, Validation. **Soheil Salahshour:** Methodology, Investigation, Funding acquisition, Formal analysis, Data curation, Conceptualization.

Ethics approval and consent to participate

Not applicable.

Consent for publication

Not applicable.

Declaration of Generative AI and AI-assisted technologies in the writing process

During the preparation of this manuscript, the authors used ChatGPT (OpenAI) and Grammarly to improve its readability, grammar, language, and overall clarity. These AI-assisted tools were used solely to support language editing and improve the text's presentation. They were not used to generate scientific ideas, interpret results, perform analyses, or draw scientific conclusions. Following the use of these tools, the authors carefully reviewed, revised, and verified all content and accept full responsibility for the accuracy, originality, and integrity of the final published manuscript.

Funding

This research received no external funding.

Declaration of Competing Interest

The authors declare that they have no known competing financial interests or personal relationships that could have appeared to influence the work reported in this paper.

Acknowledgments

Not applicable.

Data availability

No data was used for the research described in the article.

References

[1] Z. Wang, Y. Li, Layer pattern thermal design and optimization for multistream plate-fin heat exchangers—a review, Renew. Sustain. Energy Rev. 53 (2016) 500–514, https://doi.org/10.1016/j.rser.2015.09.003.
[2] G. Liao, Z. Li, F. Zhang, L. Liu, J. E, A review on the thermal-hydraulic performance and optimization of compact heat exchangers, Energies 14 (19) (2021) 6056, https://doi.org/10.3390/en14196056.
[3] Q. Wang, S. Zhang, T. Guo, W. Sha, K. Li, Z. Liu, Enhancing plate-fin heat exchanger hydraulic thermal performance through air-side fin optimization based on pseudo-3D topology optimization, Appl. Therm. Eng. 252 (2024) 123642, https://doi.org/10.1016/j.applthermaleng.2024.123642.
[4] N. Chouchane, H. Chouchane, Experimental correlations for Nusselt number and friction factor in a flat solar air collector equipped with triangular-rectangular ribs, Int. J. Heat. Fluid. Flow. 115 (2025) 109860, https://doi.org/10.1016/j.ijheatfluidflow.2025.109860.
[5] C. Nguyen, F. Desgranges, G. Roy, N. Galanis, T. Maré, E. Boucher, H.A. Mintsa, Temperature and particle-size dependent viscosity data for water-based nanofluids–hysteresis phenomenon, Int. J. Heat. Fluid Flow 28 (6) (2007) 1492–1506, https://doi.org/10.1016/j.ijheatfluidflow.2007.02.004.
[6] D. Huang, Z. Wu, B. Sunden, Pressure drop and convective heat transfer of Al2O3/water and MWCNT/water nanofluids in a chevron plate heat exchanger, Int. J. Heat. Mass. Transf. 89 (2015) 620–626, https://doi.org/10.1016/j.ijheatmasstransfer.2015.05.082.
[7] B.C. Pak, Y.I. Cho, Hydrodynamic and heat transfer study of dispersed fluids with submicron metallic oxide particles, Exp. Heat. Transf. Int. J. 11 (2) (1998) 151–170, https://doi.org/10.1080/08916159808946559.
[8] F. Afshari, A.D. Tuncer, A. Sözen, H.I. Variyenli, A. Khanlari, E.Y. Gürbüz, A comprehensive survey on utilization of hybrid nanofluid in plate heat exchanger with various number of plates, Int. J. Numer. Methods Heat. Fluid Flow 32 (1) (2022) 241–264, https://doi.org/10.1108/HFF-11-2020-0743.
[9] M.A. Al-Obaidi, F.L. Rashid, M.K. Rasheed, H.S.S. Aljibori, H.I. Mohammed, A. J. Mahdi, S. Ahmad, K. Al-Farhany, I.M. Mujtaba, Recent achievements in heat transfer enhancement with hybrid nanofluid in heat exchangers: a comprehensive review, Int. J. Thermophys. 45 (9) (2024) 133, https://doi.org/10.1007/s10765-024-03428-x.
[10] A. Bhattad, V. Atgur, B.N. Rao, N. Banapurmath, T. Yunus Khan, C. Vadlamudi, S. Krishnappa, A. Sajjan, R.P. Shankara, N. Ayachit, Review on mono and hybrid nanofluids: preparation, properties, investigation, and applications in IC engines and heat transfer, Energies 16 (7) (2023) 3189, https://doi.org/10.3390/en16073189.
[11] S. Almurtaji, N. Ali, J.A. Teixeira, A. Addali, On the role of nanofluids in thermal-hydraulic performance of heat exchangers—a review, Nanomaterials 10 (4) (2020) 734, https://doi.org/10.3390/nano10040734.
[12] M. Tekir, Experimental study on the thermal performance of hybrid nanofluid in a compact plate heat exchanger under the influence of a magnetic field, Case Stud. Therm. Eng. 69 (2025) 106031, https://doi.org/10.1016/j.csite.2025.106031.
[13] P.R. Patel, K.V. Modi, S.K. Patel, Experimental study of mono and hybrid nanofluids on square pyramid solar still, Environ. Sci. Pollut. Res. 32 (2) (2025) 693–724, https://doi.org/10.1007/s11356-024-35619-2.
[14] M. Babaelahi, Enhancing energy efficiency of plate-tube and fin heat exchangers through thermo-hydraulic optimization using advanced nanofluids for low-carbon heating systems, Proc. Inst. Mech. Eng. Part C J. Mech. Eng. Sci. 239 (18) (2025) 7657–7670, https://doi.org/10.1177/09544062251337552.
[15] F. Aktas, E.A. Elibol, O. Ulucak, A.E. Aksoy, N. Karabulut, E. Cakmak, O. Turgut, Thermal performance evaluation of Al2O3–water nanofluids in automotive radiators using ANN and PINN approaches, J. Therm. Anal. Calorim. (2025) 1–19, https://doi.org/10.1007/s10973-025-14722-7.
[16] F. Montazerifar, O.A. Akbari, S.M. Javadpour, Multi-optimization of nanofluid and fractal fin in the plate heat exchanger using RSM and TOPSIS, Energy Convers. Manag. X (2025) 101474, https://doi.org/10.1016/j.ecmx.2025.101474.
[17] R. Dhivagar, A. Sathishkumar, P. Dhamodharan, R. Prabakaran, S.C. Kim, Investigations of partial flow behavior on R290 condensation under variable heat loads in a plate heat exchanger for battery thermal management, Int. Commun. Heat. Mass. Transf. 172 (2026) 110377, https://doi.org/10.1016/j.icheatmasstransfer.2025.110377.

[18] Qian Li, Qi Zhan, Shipeng Yu, Jianchuang Sun, Weihua Cai, Study on thermal-hydraulic performance of printed circuit heat exchangers with supercritical methane based on machine learning methods, Energy 282 (2023) 128711, https://doi.org/10.1016/j.energy.2023.128711.
[19] Mathkar A. Alharthi, Bandar Awadh Almohammadi, M.A. Sharafeldin, Mohamed T. Abdelghany, Samir Bendoukha, H.A. Refaey, Heat transfer and pressure drop of Al2O3/water nanofluid in conically coiled tubes: experimental and artificial neural network prediction, Case Stud. Therm. Eng. 54 (2024) 104043, https://doi.org/10.1016/j.csite.2024.104043.
[20] A.M. Alklaibi, Kotturu V.V.Chandra Mouli, L.Syam Sundar, Heat transfer, and friction factor of Fe3O4–SiO2/water hybrid nanofluids in a plate heat exchanger: experimental and ANN predictions, Int. J. Therm. Sci. 195 (2024) 108608, https://doi.org/10.1016/j.ijthermalsci.2023.108608.
[21] Adeola Borode, Thato Tshephe, Peter Olubambi, Mohsen Sharifpur, Josua Meyer, Effects of temperature and nanoparticle mixing ratio on the thermophysical properties of GNP–Fe2O3 hybrid nanofluids: an experimental study with RSM and ANN modeling, J. Therm. Anal. Calorim. 149 (10) (2024) 5059–5083, https://doi.org/10.1007/s10973-024-13029-3.
[22] Z.Y. Aksöz, M.E. Günay, M. Aziz, K.M. Tunç, Machine learning analysis of thermal performance indicator of heat exchangers with delta wing vortex generators, Energies 17 (6) (2024) 1380.
[23] Devireddy Sandhya, Thembelani Sithebe, Veeredhi Vasudeva Rao, Relative Thermo-Hydraulic Performance of Mono and Hybrid Transformer Nanofluid in a Plate Fin Heat Exchanger-An Experimental Study, Adv. Mech. Mater. Eng. 43 (1) (2026) 43–54, https://doi.org/10.7862/rm.2026.4.
[24] A. Zell, Simulation neuronaler netze. Simulation neuronaler Netze, Oldenbourg Wissenschaftsverlag, 1994.
[25] J. Schmidhuber, Deep learning in neural networks: an overview, Neural Netw. 61 (2015) 85–117, https://doi.org/10.1016/j.neunet.2014.09.003.
[26] A. Ayub, I. Ahmad, A. Qazi, H. Sethi, M. Zulkefal, A. Zulfiqar, W. Deebani, Machine learning in heat exchangers: state-of-the-art review, ACS Eng. Au 6 (2) (2026) 231–248, https://doi.org/10.1021/acsengineeringau.5c00073.
[27] M. Rashidi, O.A. Bég, A.B. Parsa, F. Nazari, Analysis and optimization of a transcritical power cycle with regenerator using artificial neural networks and genetic algorithms, Proc. Inst. Mech. Eng. Part. A J. Power Energy 225 (6) (2011) 701–717, https://doi.org/10.1177/0957650911407700.
[28] S. Kumar, K. Veer, S. Kumar, Current trends in feature extraction and classification methodologies of biomedical signals, Curr. Med. Imaging 20 (1) (2024) E090323214502, https://doi.org/10.2174/1573405619666230309103435.
[29] R.V. Kumar, M. Alsulami, I. Sarris, G. Sowmya, F. Gamaoun, Stochastic Levenberg–Marquardt neural network implementation for analyzing the convective heat transfer in a wavy fin, Mathematics 11 (10) (2023) 2401, https://doi.org/10.3390/math11102401.
[30] H.B. Demuth, M.H. Beale, Neural Network Toolbox User's Guide, MathWorks, Incorporated, 1992.
[31] T. Butash, and L. Davisson, An overview of adaptive linear minimum mean square error predictor performance. pp. 1472-1476. https://doi.org/10.1109/CDC.1986.267114.
[32] K. Das, J. Jiang, and J. Rao, Mean squared error of empirical predictor, 2004. https://doi.org/10.1214/009053604000000201.
[33] A.G. Asuero, A. Sayago, A. González, The correlation coefficient: an overview, Crit. Rev. Anal. Chem. 36 (1) (2006) 41–59, https://doi.org/10.1080/10408340500526766.
[34] T.O. Hodson, Root mean square error (RMSE) or mean absolute error (MAE): when to use them or not, Geosci. Model. Dev. Discuss. 2022 (2022) 1–10, https://doi.org/10.5194/gmd-15-5481-2022.